The Point Spread Function of the Reflection Grating Spectrometer

Joshua Spodek, Jean Cottam, Steve Kahn, Andy Rasmussen
Columbia Astrophysics Laboratories

Bert Brinkman, Cor de Vries, Jan-Willem den Herder, Frits Paerels
Space Research Organization of the Netherlands

Graziella Branduardi-Raymont
Mullard Space Science Laboratory

ABSTRACT

X-ray calibrations of the individual reflection grating elements in the Reflection Grating Array at Columbia/Nevis Labs and the full arrays at MPE/Panter have yielded both the efficiency and spectral resolution information necessary for a detailed, comprehensive understanding of the Reflection Grating Spectrometer.

All gratings have surface irreguliarities such as nonflatness and micro-roughness. These surface properties, along with as-built deviations from the ideal array design, broaden the monochromatic point spread function. A new extrapolation of scalar scattering theory, constrained by measurement, is used to predict angular redistribution functions by the diffraction grating elements. Comparison of Panter measurements with the results of a fully detailed raytrace, based on the scattering theory and assembly room metrology, is used to verify as-built grating positions in both RGA flight models

1. The Physical Model

We have developed a fully detailed physical model of the XMM RGS. This model incorporates all the RGS hardware and simulates the various known processes that have observable effects on the point spread function of the RGS. Each of these modeled effects has been tested or measured independent of and prior to the RGS calibration program at MPE/Panter. As a result, the model contains no free parameters. Documentation of these measured external constraints to the model are available at *http://astro1.nevis.columbia.edu/xmm/documents*. (Note that due to an assembly-time error in an interferometer that was not discovered until after assembly, the model for RGS2/RGA1 only actually does contain one unrecoverable parameter which had to be fitted.)

This section first presents a brief description of the physical hardware and processes on which the model is based. The following section presents a table describing the sources of constraint for each component or process described in this section.

At a component level, the elements that had to be modeled were fourfold: the telescope mirror module, single grating scatter, the Reflection Grating Array on a grating-level basis, and the calibration alignment geometry.

Modeling of the telescope mirror module was based on the nominal paraboloid and hyperboloid figure parameters. Though detailed information was available for deviations from nominal figures, these discrepancies were found to be adequately modeled by a Lorentzian distribution of slope perturbations. Furthermore, optical axis misalignments for the 58 shells were empirically parametrized.

Single grating scatter was modeled according to a new extension of scalar diffraction theory to reflection gratings (Paerels; Spodek). This theory predicts X-ray scattering due to fluctuations from the ideal grating surface. For PSF analysis, only scattering to small angles about the spectral orders was incorporated into the model. The theory for small angle grating scatter predicts the shape of the scattering wings about the core as well as the fraction of light going into those wings. This theory depends on two input parameters for each grating surface: σ, the root mean square height of surface fluctuations from ideal, and l, the correlation length of surface fluctuations.

Modeling of the Reflection Grating Array on a grating-level basis incorporated mechanical tolerances of the fabrication of the integrating structure and the assembly room grating-to-grating alignment. Modeling of the grating-to-grating alignment incorporated grating tilt relative to the ideal alignment angle, grating position relative to nominal, grating twist relative to flat (untwisted), grating figure relative to flat (unbowed), and (in the case of RGS2/RGS1) the interferometer misalignment.

Calibration alignment involved modeling of the Reflection Grating Array on an array-level basis and modeling the input source spectrum. The RGA (on an array-level basis) had to be positioned in six dimensions. Modeling the source spectrum involved understanding line widths and satellite line structure, which could be modified by the solid state conditions of the source, as well as the properties of the monochrometer when it was used.

2. Calibration

Each input parameter to the physical model was constrained by independent measurement. The table below briefly describes how each parameter was determined. Once all of these sources were input to the model, there remained no further adjustable parameters. Accordingly, the comparisons of the model predictions with the MPE/Panter data in the next section should be regarded as just that: a comparison of our understanding of the entire Reflection Grating Spectrometer with the actual RGS. No fitting was performed to obtain these plots.

Constraints of Physical Model Input Parameters

Process or Component	Subprocess or Subcomponent	Source of Constraint of Input Parameter
Telescope Mirror Module	Figure parameters	Metrology performed at MSSL
	Slope distribution and optical axis coalignment	EPIC non-RGS MPE/Panter calibration
Single Grating Scattering Theory	Testing of new theory	Verification performed on subsample of gratings over wide range of parameter space at Columbia's Nevis Lab's Longbeam facility
	Individual grating scattering parameters	σ and l determined for each of 362 gratings.
Reflection Grating Array	Integrating structure mechanical tolerances	Specified to each supplier and verified
	Grating Alignment (tilt, position, twist, figure)	Interferometrically determined for each grating during assembly
	RGS2/RGA1 interferometer assembly misalignment error	Discovered and modeled during MPE/Panter calibration program; unrecoverable parameter fitted with calibration data from Panter
Calibration alignment	Hardware positions	Mirror Module, RGA, and RFC positions measured with theodolite. Post-calibration redundancy software checks developed and performed.
	Theodolite reproducibility and consistency	Dedicated pre- and post- calibration measurements performed at MPE/Panter for each run.
	Source spectra	Parameters determined from EOBB (single grating) test and AXAF calibration tests

3. Model/Data Comparisons

Two sets (one for RGS1/RGA2, one for RGS2/RGA1) of typical comparisons between the prediction of the physical model and the results of the calibration testing are displayed below. They graphically display the extent to which our knowledge of the RGS overlaps the true physical system.

Small wavelength, high order data provided greater diagnostic power for pre-flight calibration since short wavelength lines are intrinsically narrower than the RGS core. These lines were preferably used, therefore, despite lying outside the likely useful range in orbit. The Mg K line here, at $\lambda = 9.89$ Å, scatters 53% of first order and 65% of third order light into small angles about its core. It also contains a nearby satellite line ($\Delta\lambda = 7 \times 10^{-2}$) which is resolved by second order.

The two sets of four orders each (zero through third order) are presented alternately with linear and logarithmic scaling in order to visually accent the core or wings.

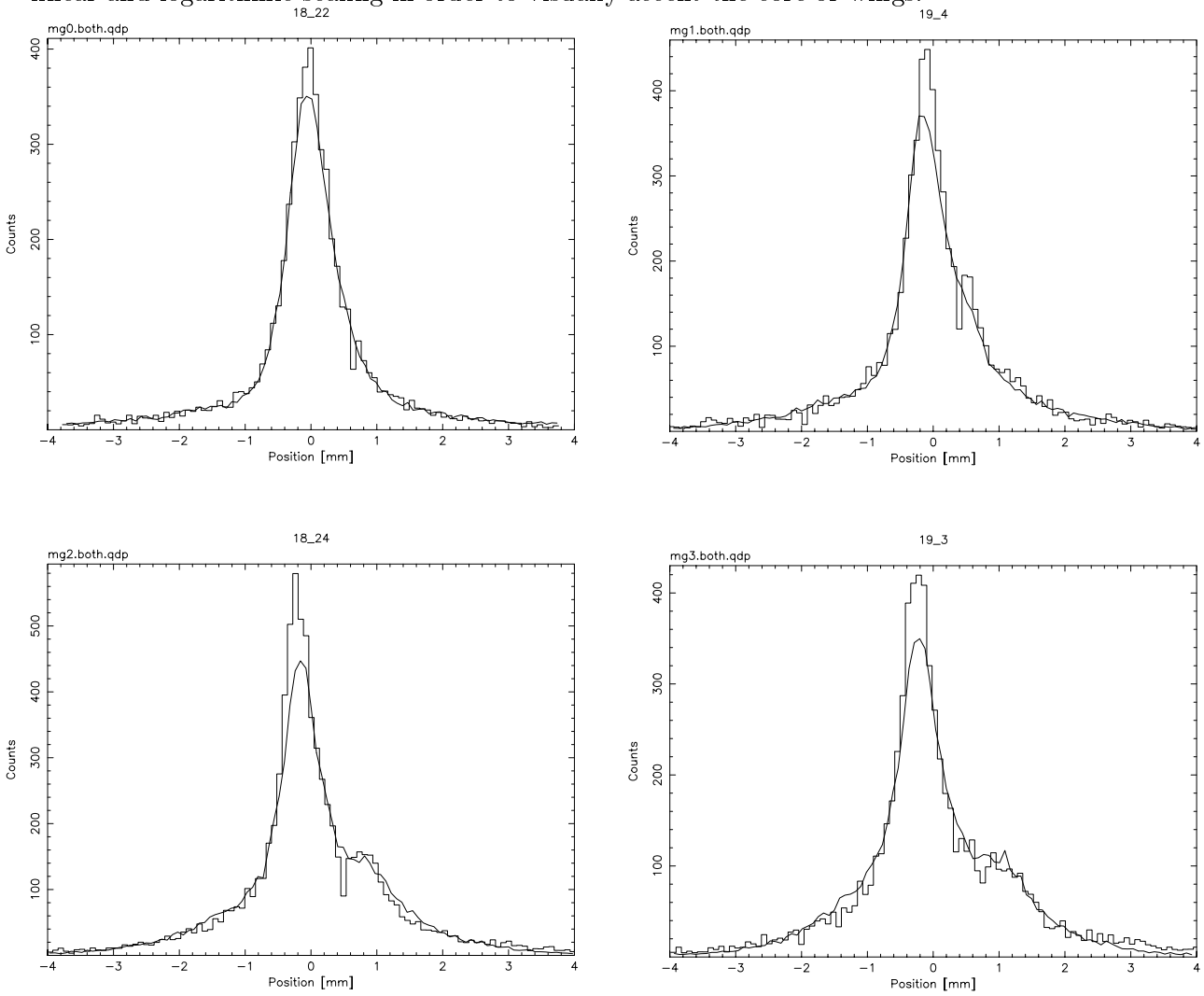

Fig. 1.— The RGS2/RGA1 (first-built array) profiles with linear scaling

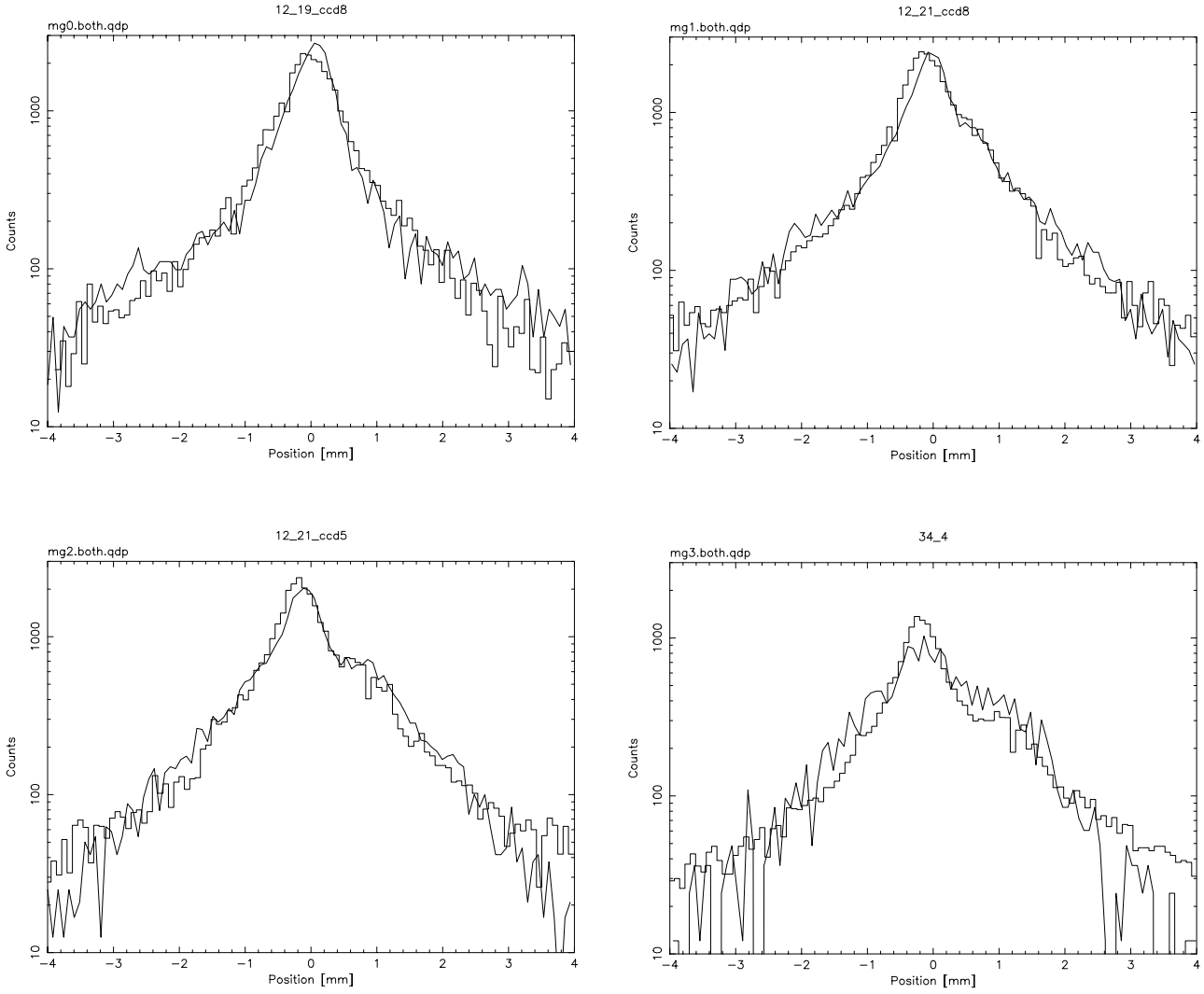

Fig. 2.— The RGS1/RGA2 (second-built array) profiles with logarithmic scaling to accent scattering wings

4. Predicted Performance

The predicted performance of the RGS is best parametrized by the resolution ($\Delta\lambda$) and the resolving power ($\lambda/\Delta\lambda$) as functions of wavelength. The eight plots below display these numbers first for RGS2/RGA1, then for RGA1/RGS2.

For each RGS the line width, $\Delta\lambda$, is measured alternately as Half Energy Width (HEW) and Full Width at Half Maximum (FWHM). The HEW is generally more useful for measuring the sensitivity of weak line features. The FWHM is generally more quoted to describe the ability of a spectrometer to separate two closely spaced spectral lines.

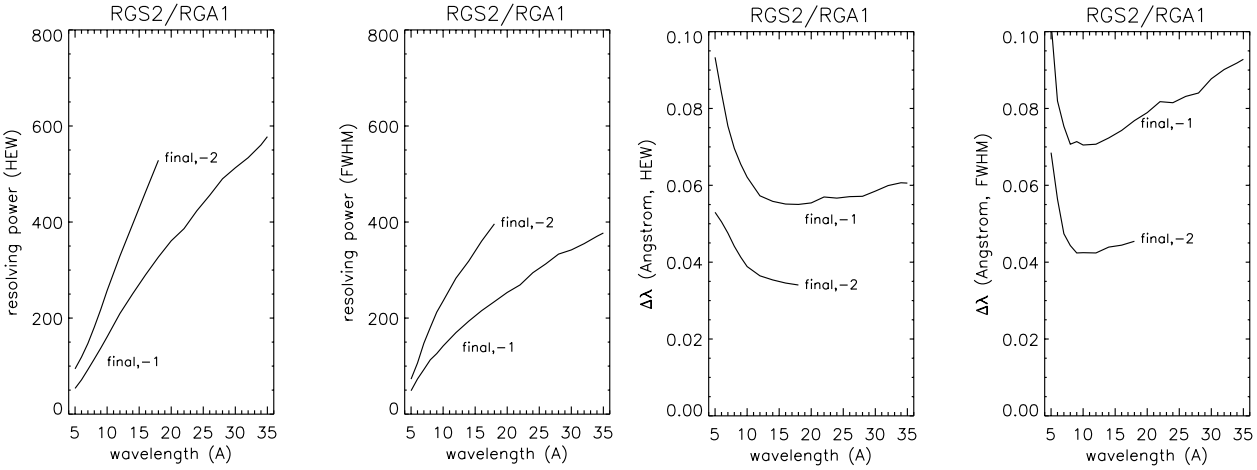

Fig. 3.— First built grating array, resolution degraded by interferometer error during assembly

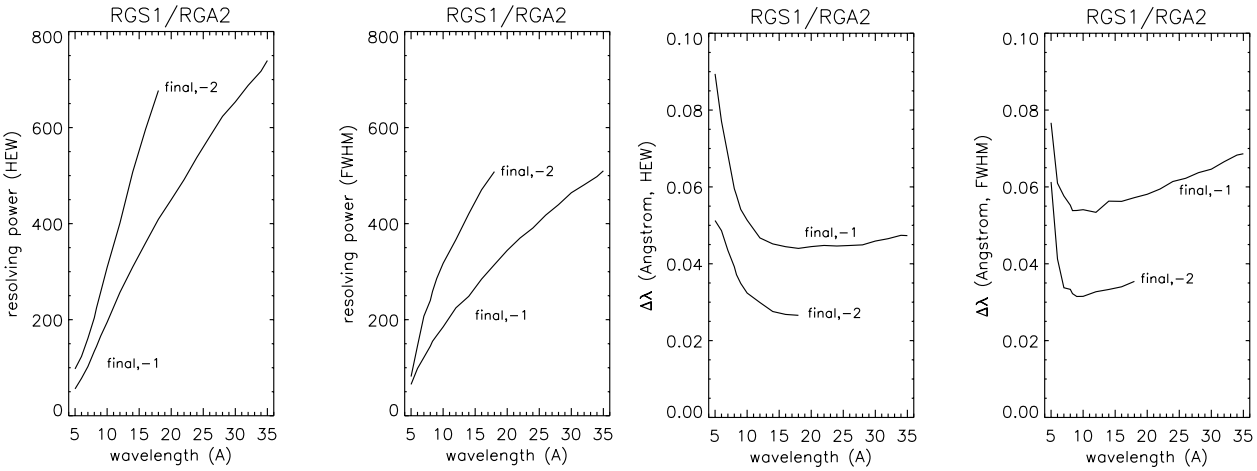

Fig. 4.— Second built grating array

REFERENCES

Paerels, F., et al 1994, Proc. SPIE, 2283, 107

Spodek, J., et al, in preparation